Analyst

Quantitative Surface-Enhanced Raman Spectroscopy Chemical Analysis using Citrate as an in-situ Calibrant

Journal:	*Analyst*
Manuscript ID	AN-ART-11-2018-002170.R1
Article Type:	Paper
Date Submitted by the Author:	29-Dec-2018
Complete List of Authors:	Salemmilani, Reza; University of California Santa Barbara, Mechanical Engineering Mirsafavi, Rustin; University of California Santa Barbara, Institute for Collaborative Biotechnologies Fountain, Augustus; Edgewood Chemical Biological Center, Research and Technology Moskovits, Martin; University of California, Chemistry and Biochemistry 9510 Meinhart, Carl; University of California, Santa Barbara, Department of Mechanical Engineering

Quantitative Surface-Enhanced Raman Spectroscopy Chemical Analysis using Citrate as an *in-situ* Calibrant

Reza Salemmilani,[†,‡] Rustin Y. Mirsafavi,[§,‡] Augustus W. Fountain, III,[⊥] Martin Moskovits,[▽] Carl D. Meinhart[†,*]

[†]Department of Mechanical Engineering, University of California Santa Barbara, Santa Barbara, California 93106, United States

[§]Department of Biomolecular Science and Engineering, University of California Santa Barbara, Santa Barbara, California 93106, United States

[⊥]Edgewood Chemical and Biological Center, Edgewood, Maryland 21010, United States

[▽]Department of Chemistry and Biochemistry, University of California Santa Barbara, Santa Barbara, California 93106, United States

[‡]Equal contribution authors

*address correspondence to: meinhart@ucsb.edu

ABSTRACT

Direct detection, or inferring the presence of illicit substances, is of great forensic and toxicological value. Surface-enhanced Raman spectroscopy (SERS) has been shown capable of detecting such molecules in a quick and sensitive manner. Herein we describe an analysis strategy for quantitation of low concentrations of three analytes (methamphetamine, cocaine, and papaverine) by SERS analysis using the citrate capping agent that initially saturates the silver nanoparticles' surface as an *in-situ* standard. The citrate is subsequently displaced by the analyte to an extent dependent on the analyte's concentration in the analyte solution. A general model for the competitive adsorption of citrate and a target analyte was developed and used to determine the relative concentrations of the two species coexisting on the surface of the silver nanoparticles. To apply this model, classical least squares (CLS) was used to extract the relative SERS contribution of each of the two species in a given SERS spectrum, thereby accurately determining the analyte concentration in the sample solution. This approach, in essence, transforms citrate into a local standard against which the concentration of an analyte can be reliably determined.

INTRODUCTION

Precise determination of the concentration of narcotic drugs in a sample is crucial to our understanding, control, and policing of drug use, trafficking, and production. Many techniques are available for detecting the presence of such substances either directly, or indirectly by determining, for example, drug metabolites or residues. When choosing between a direct or indirect analytical target, the capabilities of the analytical system must roughly match the anticipated results, which normally means determining the identity of the drug and its concentration. SERS has been shown to be capable of identifying a wide range of molecules at low concentrations.[1-9]

Nanostructured metals are commonly used as the SERS substrates on which such measurements are carried out. These have been produced in a variety of forms such as colloidal nanoparticles, fixed

nanoparticles, and nanofabricated substrates.[10, 11] Colloidal metal nanoparticles are among the most prevalent materials used for SERS measurements in which, most of the SERS signal normally arises from nanoparticle aggregates in which the interstices function as so-called SERS "hot spots" where the enhanced optical fields and, consequently, the SERS signals from molecules occupying such hot spots are thought to be especially intense.[12] Nanoparticle aggregation is often induced by a chemical agent, such as lithium chloride, that by displacing the capping agent, disrupts the electrostatic and steric repulsive forces created by the capping agents, responsible for nanoparticles' stability in solvents.[13]

Solvent molecules and other molecules that may be present in addition to the targeted analyte can also contribute to the SERS signal, often making identification and quantification of the target chemical species difficult. Moreover, factors such as fluctuations in laser power, degree of aggregation of the SERS-active colloid, pH of the solution, and temperature, may influence the intensity of the acquired SERS signal.[8, 14] Studies have reported analyte quantification by using, for example, isotope-edited internal standards,[15, 16] labelling the analyte,[17] adding exogenous species such as salts as internal standards,[18, 19] or by attempting to quantify the plasmonic enhancement of the SERS substrate.[18, 20]

A common capping agent that stabilizes silver nanoparticles (AgNP) is citrate, a remnant of the reduction process through which the silver colloid was synthesized.[21, 22] Recently, Park and Shumaker-Parry have characterized, in detail, the role of citrate in stabilization of gold nanoparticles, demonstrating that citrate anions stabilize nanoparticles by a combination of electrostatic and steric mechanisms.[13] Most commercially-available AgNPs are citrate-capped, which are particularly useful for SERS applications because citrate anions, unlike capping agents such as polyvinylpyrrolidone (PVP), are displaceable by a wide range of analytes. However, citrate produces intense and potentially interfering SERS signals of its own, and, when not fully displaced, as happens with many analytes, establishes a surface equilibrium with the analyte, which contaminates the SERS signal, while reducing the ability of the substrate to accommodate the target species. We show that this effect can be turned to

one's benefit by using the analyte/citrate surface equilibria as a calibration technique for producing analyte calibration curves which can be used to confidently determine analyte concentration.

By using a microfluidic device one can also exploit the diffusion-dominated laminar flow regime providing ample time for the analyte and citrate to establish ibrium before the SERS analysis is carried out downstream in the channel. Limits of detection using this microfluidic device are determined for the analytes methamphetamine, cocaine, and papaverine. Classical least squares (CLS) chemometrics is used to quantify the relative contributions of the analyte and citrate. Finally, a surface kinetics model is derived on the basis of which a calibration curve is computed for each of the three analytes, reliably relating the analyte and citrate SERS signal intensities to the analyte concentration in solution.

EXPERIMENTAL

The microfluidic device was constructed in a flow-merging arrangement that unites three inlet laminar flows: AgNPs, LiCl (an aggregation agent), and analyte solutions into a single channel with a single outlet (Figure 1).[23, 24] Laminar flow is critical to the device's operation allowing cross-stream transport to occur only through diffusion. Standard soft-lithography was used,[25, 26] in which uncured liquid polydimethylsiloxane (PDMS, Dow Corning Sylgard 184) was poured onto a silicon wafer with SU-8 epoxy photoresist hills patterned with the desired features. The PDMS was cured in an oven at 80°C for 1.5 hours. The PDMS layer was then removed and cut to fit a regular 25 mm by 75 mm glass slide in which fluidic vias had been drilled. The microfluidic channels were 20 µm deep by 50 µm wide. PDMS and glass were then exposed to ozone for 10 minutes and pressed into contact creating a permanent seal.

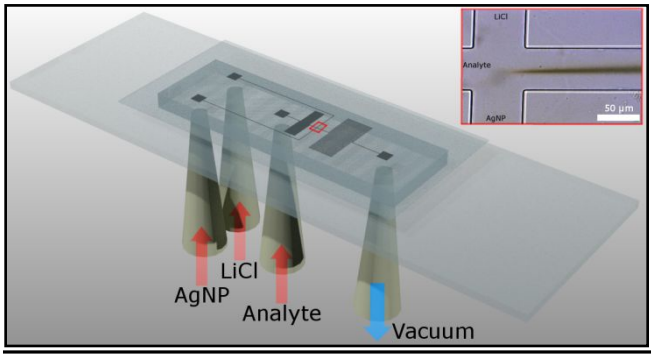

Figure 1: Rendering of a fully fabricated microfluidic device. Cut out shows a magnified image of an operating device. The dark streak in the middle of the outlet channel depicts aggregation of AgNPs downstream of the junction. Red arrows demark the inlets while the blue arrow demarks the outlet.

The device was loaded with 20 µL of 0.02 mg mL^{-1} 40 nm AgNPs (NanoXact, nanoComposix) and 20 µL of 0.2 M LiCl (Sigma-Aldrich, Merck KGaA) in the respective flanking inlets. The center inlet was loaded with fluid containing various concentrations of methamphetamine, cocaine, or papaverine (Sigma-Aldrich, Merck KGaA). The channels were then primed up to the merging junction with positive pressure from a syringe, then operated by applying vacuum to the outlet, allowing flow for at least 2 minutes before raster scanning a 50 µm × 100 µm portion of the channel using the Raman microscope (HORIBA, Ltd.) to locate a strong SERS signal. SERS interrogation was carried out using a 633 nm laser at a power of 83 µW beginning 100 µm downstream of the junction. A 50x objective lens was used, and each point was exposed to the laser for two seconds.

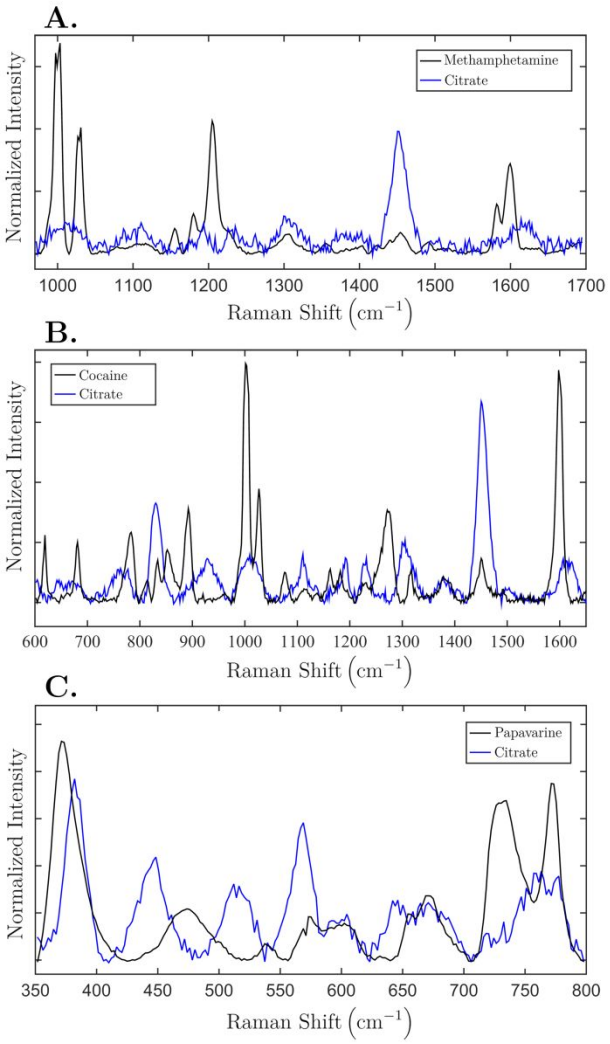

Figure 2: CLS loadings of methamphetamine (A), cocaine (B), and papaverine (C), in which citrate spectra are also included. Preprocessing consisted of baselining and normalization by the area under the spectra.

The collected data were analyzed with PLS toolbox (Eigenvector Research Inc.) using the classical least squares module. Model spectra (loadings) were collected for each analyte, and for citrate. The analyte loadings spectra were collected using freshly prepared borate-capped AgNPs and high concentration analyte solutions (> 3 mM) in a device. Citrate loading spectra were collected using deionized MilliQ water (18.2 MΩ·cm) as the analyte in a device using citrate-capped AgNPs. The preprocessed loadings in the CLS model are shown in Figure 2.

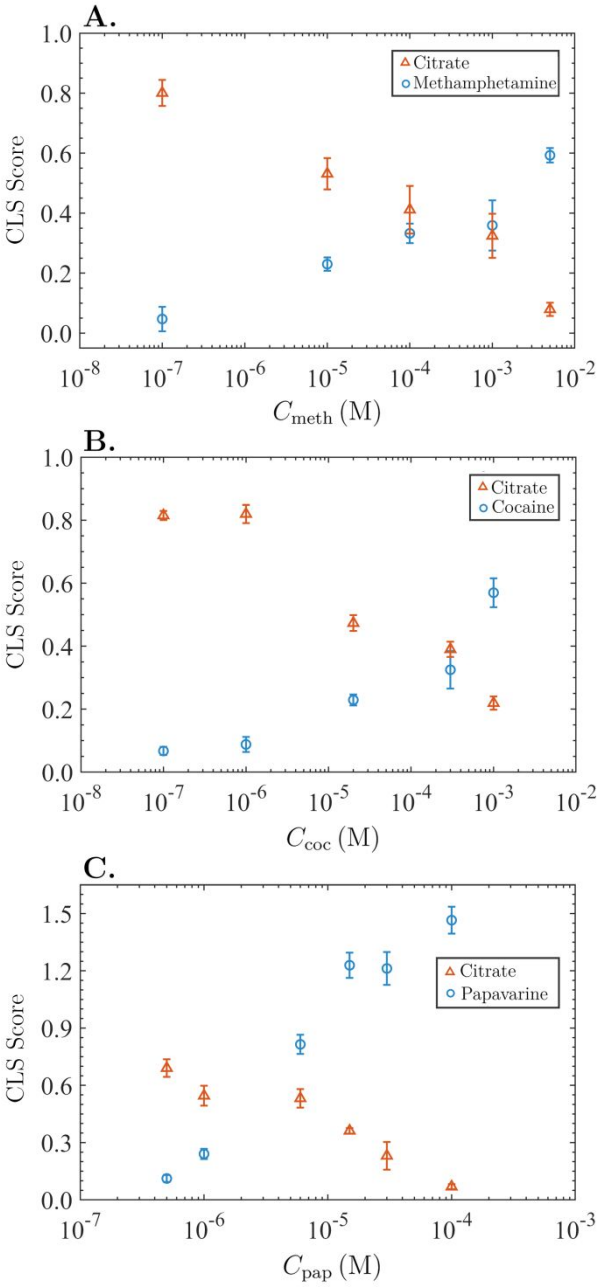

Figure 3: CLS scores for the SERS spectra of methamphetamine (A), cocaine (B), papaverine (C), and citrate as a function of analyte concentration. 95% confidence intervals are shown for each data point.

Raw spectra acquired from serially-diluted analyte samples were processed as follows: Only spectra with intense bands at approximately 229 cm^{-1} (Figure S-1), characteristic of AgNPs aggregates were included in the analysis. The 229 cm^{-1} band corresponds to an Ag-Cl vibration indicating the addition of lithium, sodium, or potassium chloride aggregating agent.[23, 27, 28] Spectra collected from the regions in the microfluidic channel with no aggregates were not analyzed. Spectra were baselined using an automatic Whittaker filter, followed by normalization by the area under the spectrum in the wavenumber ranges shown in Figure 2. Preprocessed spectra were then fitted using the CLS model and relative contributions of citrate and the analyte to the spectra were calculated.

RESULTS AND DISCUSSION

The spectral loadings that were used for CLS model generation resembled typical spectra reported in the literature.[2, 3, 6, 10, 23] The spectral regions that were selected for analysis (Figure 2) were chosen to improve the discrimination between the citrate background, while capturing the dominant Raman modes of the analytes. For each analyte (methamphetamine, cocaine, and papaverine) a series of spectra were collected at various concentrations. Concentrations of analytes were decreased by dilution

until no significant score of the analyte was returned by the CLS analysis. Significant scores were determined as having a CLS score greater than two standard deviations above the mean score of the negative control sample (DI H_2O). A major advantage of using CLS for quantitative analysis of Raman spectra (as opposed to comparing only one or two peaks) is that we use the entire spectrum over a large wavenumber range and use a large set of changes in relative peak heights, peak widths, relative feature intensities, etc. to improve the discrimination and relative quantification of the species that contribute to the spectra.

The limits of detection determined in this manner for methamphetamine, cocaine, and papaverine were 100 nM, 100 nM, and 500 nM, respectively. The range of concentrations of methamphetamine and cocaine detected covered the normally reported range of forensic and toxicological values.[3, 29] The concentrations of papaverine analyzed were within a forensically pertinent concentration range.[24] The scores for each concentration of analyte was calculated from a minimum of 5 spectra. The calculated scores versus concentrations are reported in Figure 3. A similar trend is observed for each analyte, with the citrate score decreasing as the analyte concentration increases, implying that the analyte displaces citrate off the AgNPs and into solution. Chloride anions from LiCl are assumed to initially occupy a certain fraction of adsorption sites on the silver surfaces, which make those sites inaccessible to both the analyte and citrate over the duration of the test. The quantity of citrate displaced from the surface of the AgNPs was (not unexpectedly) found to be a function of (i) the concentration of the analyte, and (ii) the competitive affinity of the analyte versus citrate for silver surfaces. Qualitatively, it is clear that papaverine has a lower affinity for the AgNPs than either cocaine or methamphetamine. Its lowest detectable concentration was 500 nM, while each of the two other analytes had limits of detection lower by approximately a factor of five. We also show that papaverine has a lower propensity to displace citrate from the Ag surfaces than methamphetamine and cocaine.

In order to acquire a better understanding of our observations and to facilitate the quantitative determination of the unknown concentration of a collected sample, we develop a model that yields a

"calibration" function relating the measured SERS intensities of the adsorbed analyte and the adsorbed citrate to the concentration of the analyte in solution. In order to derive this relationship, we assume that the microfluidic system has reached a steady state after 2 minutes of flow. This assumption is justified by the observation that the Raman signal intensity reaches a plateau after 1 to 2 minutes of flow, beyond which the Raman intensity remains constant with time.

Denoting the analyte as species 1, and citrate as species 2, the rate equations describing these processes are given as follows:

$$\frac{dN_1}{dt} = k_1 c_1 (S - N_1 - N_2) - k_{-1} N_1 \quad \text{[Eq. 1] for analyte}$$

$$\frac{dN_2}{dt} = k_2 c_2 (S - N_1 - N_2) - k_{-2} N_2 \quad \text{[Eq. 2] for citrate}$$

In which N_1, k_1, c_1, k_{-1}, and S are, respectively, the number of analyte molecules on the silver surface; the adsorption rate constant of the analyte; the concentration of the analyte in solution; the desorption rate constant of the analyte; and the total number of adsorption sites on the surface. Analogous parameters for citrate are subscripted 2.

At steady state:

$$\frac{dN_1}{dt} = \frac{dN_2}{dt} = 0 \quad \text{[Eq. 3]}$$

Substituting [Eq. 1] and [Eq. 2] into [Eq. 3] yields:

$$\frac{N_1 k_{-1}}{c_1 k_1} = \frac{N_2 k_{-2}}{c_2 k_2} \quad \text{[Eq. 4]}$$

Assuming the silver surface is initially saturated with citrate and the citrate concentration in solution is initially zero, the steady-state concentration of citrate in solution (c_2) depends solely on the quantity of analyte (N_1) that adsorbs on the surface.

We propose the relationship:

$$c_2 = bN_1^n \qquad \text{[Eq. 5]}$$

In which b is a proportionality constant, and n is an analyte-specific parameter that relates the number of citrate molecules displaced per analyte molecule adsorbing on the silver surface. This depends on multiple factors, chief among them the relative size of the area occupied by an analyte molecule as compared to a citrate molecule. A large analyte molecule could displace several citrate moieties and therefore be characterized by a larger n value.

Substituting [Eq. 5] into [Eq. 4] yields:

$$\frac{N_1^{1+n}}{N_2} = \beta c_1 \qquad \text{[Eq. 6]}$$

Where $\beta = \frac{k_1\, k_{-2}}{k_{-1} k_2 b}$

Assuming the SERS signal is proportional to the number of molecules illuminated and therefore proportional to the CLS scores, one obtains:

$$\frac{S_1^{n+1}}{S_2} = \frac{\sigma_1^{n+1}}{\sigma_2}\beta c_1 \qquad \text{[Eq. 7]}$$

In which S_1 and S_2 are the SERS scores proportional to the SERS intensities of analyte and citrate, respectively, and σ_1 and σ_2 are parameters proportional to the Raman cross sections of the analyte and citrate, respectively. Because the range of concentrations (c_1) spans several orders of magnitude, we fit

our data in terms of logarithms of concentration, otherwise the low concentration results would have insignificant impact on the parameters retrieved. In passing it is worth noting that this analysis does not require precise knowledge of the initial citrate coverage on the silver nanoparticles for a useful calibration curve to be determined using the above approach.

Taking the logarithm of both sides of [Eq. 7] produces a linear plot in $\log_{10}(c_1)$:

$$\log_{10}\left(\frac{S_1^{n+1}}{S_2}\right) = \log_{10}(c_1) + B \qquad \text{[Eq. 8]}$$

where $B = \log_{10}\left(\frac{\sigma_1^{n+1}}{\sigma_2}\beta\right)$

The scores of citrate and scores of the analytes were randomly resampled with replacement (bootstrapped) with 5000 iterations to increase statistical robustness. The scores of citrate, scores of the analytes, and concentrations of analyte were then fitted using [Eq. 8], optimizing by using n and B as adjustable parameters. The exponent values returned by the fit for methamphetamine, cocaine, and papaverine were 4.19, 3.77, and 1.20, respectively. The calculated data as well as the calibration curve equations for each analyte are presented in Figure 4. Note that the exponents on the Raman scores for methamphetamine and cocaine are more than twice that for papaverine, in agreement with the magnitudes of the Raman cross-sections for those species relative to that of citrate shown in Figure 2.

It is evident from Fig 4 that the combination of CLS chemometrics and competitive adsorption modelling is quite powerful for constructing concentration calibration curves over a wide dynamic range (nanomolar to millimolar). The sensitivity of the technique is evident. It is however desirable to ascertain the selectivity of the model for the analyte of interest. Selectivity of the CLS models are characterized by applying each model to all three analytes and comparing the residuals after the CLS fit is performed. Q-residuals are used for quantifying the fraction of the spectrum that is not accounted for

by the CLS model. Q-residuals indicate how well a spectrum conforms to its projection onto the CLS model; The lower the value of the Q-residuals, the better the CLS model suited the data.

Figure 5 shows the Q-residuals for all three models. As seen in the figure, when the CLS model is applied to the appropriate analyte, the residuals are relatively small. However, when applying the model appropriate to one analyte to another analyte, the residuals increase by at least a factor of 2. This demonstrates the selectivity of the analysis technique for the analyte of interest. It is interesting to note that the residuals for papaverine differ significantly from those of cocaine and methamphetamine. This is due to the very different Raman spectrum of papaverine from the rather similar spectra of methamphetamine and cocaine.

CONCLUSION

Citrate-capped AgNPs were used to detect methamphetamine, cocaine, and papaverine in a microfluidic device. CLS analysis was carried out on the SERS spectra of each of the analytes with high concentration analyte and citrate serving as the model spectra. From the scores of the CLS analysis, the limits of detection for the three analytes were determined. A model describing the ratio of analyte to citrate scores was formulated and used to determine the relative propensity of each analyte to displace citrate at the silver surface, and to produce calibration curves with which to determine the analyte concentration in solution based on the relative SERS intensities of the analyte to citrate.

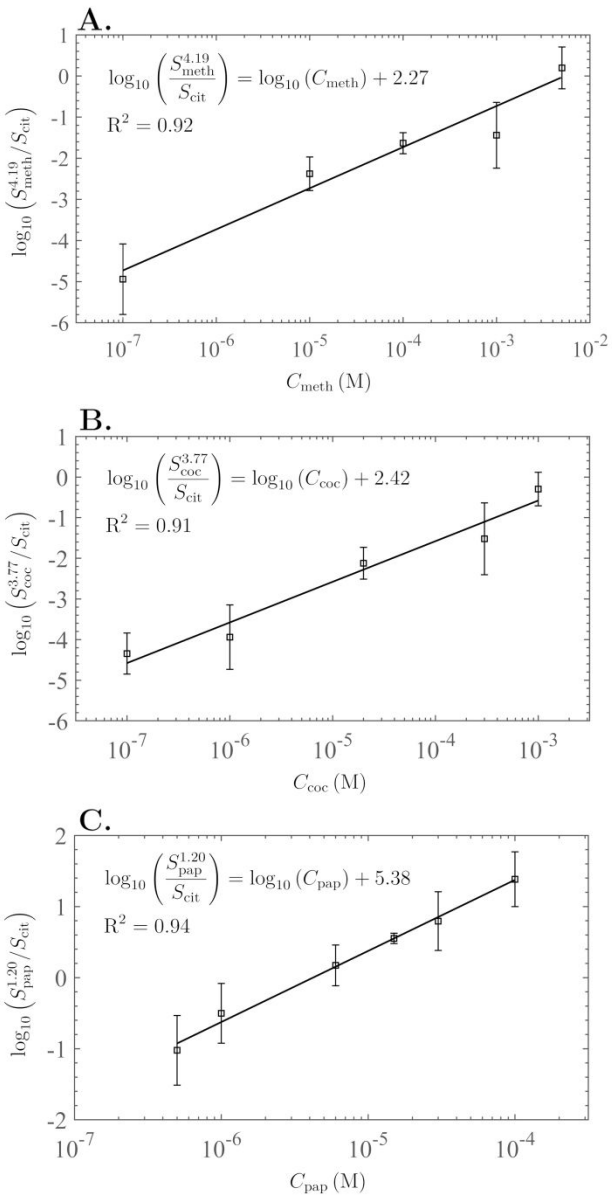

Figure 4: Calculated Raman score ratios as function of the analyte concentration for: methamphetamine (A), cocaine (B), and papaverine (C). The best fit line for each analyte is shown together with its equation and R^2 value. Error bars represent 2 standard deviations from the mean of the datapoints used for calculation of the regression lines.

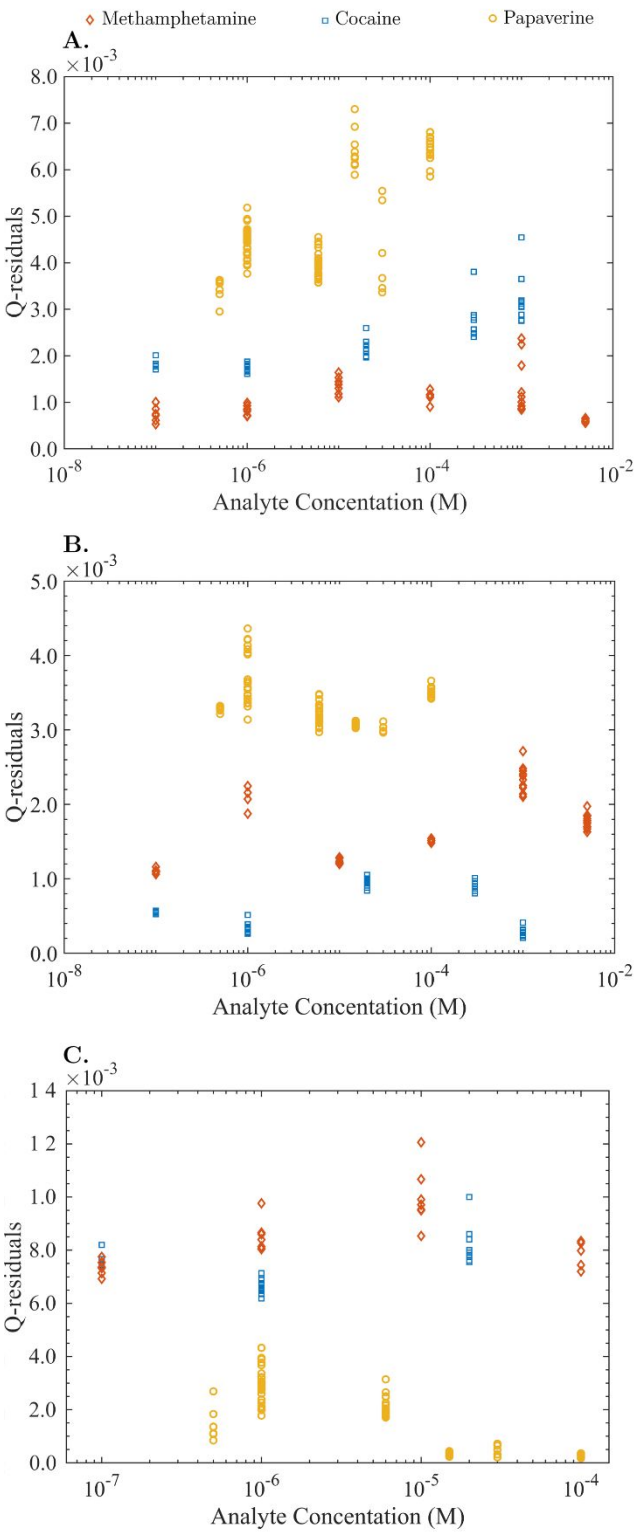

Figure 5: Q-residuals for the analytes when applied to methamphetamine model (A), cocaine model (B), and papaverine model (C). When models are applied to the analyte for which the model was constructed, residuals are low; when models are applied to the unsuitable analyte, residuals are significantly higher.

CONFLICTS OF INTEREST

There are no conflicts of interest to declare.

ACKNOWLEDGMENTS

Authors would like to thank Dr. Brian Piorek for his contributions in discussions. Funding was provided by the U.S. Army via the Forensics Applied Research Program (PE 0602622A Project 552) at the Edgewood Chemical Biological Center, and by the Institute for Collaborative Biotechnologies through grant W911NF-09-0001 from the U.S. Army Research Office. The content of the information does not necessarily reflect the position or the policy of the Government, and no official endorsement should be inferred.

Supplementary Information. Representative raw Raman spectra for experiments with each of the three analytes.

REFERENCES:

1. I. J. Jahn, O. Zukovskaja, X. S. Zheng, K. Weber, T. W. Bocklitz, D. Cialla-May and J. Popp, *Analyst*, 2017, **142**, 1022-1047.
2. R. Salemmilani, B. D. Piorek, R. Y. Mirsafavi, A. W. Fountain, 3rd, M. Moskovits and C. D. Meinhart, *Anal Chem*, 2018, DOI: 10.1021/acs.analchem.8b00510.
3. S. C. Farquharson S., Sengupta A., Huang H., Inscore F., *Pharmaceutics*, 2011, **3**, 425-439.
4. F. Inscore, C. Shende, A. Sengupta, H. Huang and S. Farquharson, *Appl Spectrosc*, 2011, **65**, 1004-1008.
5. B. D. Piorek, C. Andreou, M. Moskovits and C. D. Meinhart, *Analytical Chemistry*, 2014, **86**, 1061-1066.
6. K. R. Ackermann, T. Henkel and J. Popp, *Chemphyschem*, 2007, **8**, 2665-2670.
7. C. L. Haynes, A. D. McFarland and R. P. Van Duyne, *Analytical Chemistry*, 2005, **77**, 338a-346a.
8. E. Kammer, K. Olschewski, T. Bocklitz, P. Rosch, K. Weber, D. Cialla and J. Popp, *Phys Chem Chem Phys*, 2014, **16**, 9056-9063.
9. S. Kasera, L. O. Herrmann, J. del Barrio, J. J. Baumberg and O. A. Scherman, *Sci Rep*, 2014, **4**, 6785.
10. M. Kerker, O. Siiman, L. A. Bumm and D. S. Wang, *Appl Optics*, 1980, **19**, 3253-3255.
11. W. Li, X. Zhao, Z. Yi, A. M. Glushenkov and L. Kong, *Anal Chim Acta*, 2017, **984**, 19-41.
12. K. L. Wustholz, A. I. Henry, J. M. McMahon, R. G. Freeman, N. Valley, M. E. Piotti, M. J. Natan, G. C. Schatz and R. P. Van Duyne, *J Am Chem Soc*, 2010, **132**, 10903-10910.
13. J. W. Park and J. S. Shumaker-Parry, *J Am Chem Soc*, 2014, **136**, 1907-1921.
14. S. E. Bell and N. M. Sirimuthu, *Chem Soc Rev*, 2008, **37**, 1012-1024.
15. A. Subaihi, Y. Xu, H. Muhamadali, S. T. Mutter, Ewan W. Blanch, D. I. Ellis and R. Goodacre, *Analytical Methods*, 2017, **9**, 6636-6644.
16. A. Marz, K. R. Ackermann, D. Malsch, T. Bocklitz, T. Henkel and J. Popp, *J Biophotonics*, 2009, **2**, 232-242.
17. A. Loren, J. Engelbrektsson, C. Eliasson, M. Josefson, J. Abrahamsson, M. Johansson and K. Abrahamsson, *Anal Chem*, 2004, **76**, 7391-7395.
18. S. E. Bell, J. N. Mackle and N. M. Sirimuthu, *Analyst*, 2005, **130**, 545-549.
19. S. E. Bell and N. M. Sirimuthu, *Analyst*, 2004, **129**, 1032-1036.
20. R. W. Taylor, T. C. Lee, O. A. Scherman, R. Esteban, J. Aizpurua, F. M. Huang, J. J. Baumberg and S. Mahajan, *ACS Nano*, 2011, **5**, 3878-3887.
21. C. H. Munro, W. E. Smith, M. Garner, J. Clarkson and P. C. White, *Langmuir*, 1995, **11**, 3712-3720.
22. N. G. Bastús, F. Merkoçi, J. Piella and V. Puntes, *Chemistry of Materials*, 2014, **26**, 2836-2846.
23. C. Andreou, M. R. Hoonejani, M. R. Barmi, M. Moskovits and C. D. Meinhart, *ACS Nano*, 2013, **7**, 7157-7164.
24. R. Y. Mirsafavi, K. Lai, N. D. Kline, A. W. Fountain, 3rd, C. D. Meinhart and M. Moskovits, *Anal Chem*, 2017, **89**, 1684-1688.
25. J. C. McDonald, D. C. Duffy, J. R. Anderson, D. T. Chiu, H. Wu, O. J. Schueller and G. M. Whitesides, *Electrophoresis*, 2000, **21**, 27-40.
26. G. M. Whitesides, E. Ostuni, S. Takayama, X. Jiang and D. E. Ingber, *Annu Rev Biomed Eng*, 2001, **3**, 335-373.

27. L. Guerrini, J. V. Garcia-Ramos, C. Domingo and S. Sanchez-Cortes, *Anal Chem*, 2009, **81**, 1418-1425.
28. A. Otto, A. Bruckbauer and Y. X. Chen, *Journal of Molecular Structure*, 2003, **661-662**, 501-514.
29. R. J. Schepers, J. M. Oyler, R. E. Joseph, Jr., E. J. Cone, E. T. Moolchan and M. A. Huestis, *Clin Chem*, 2003, **49**, 121-132.

FOR TOC ONLY: